Modeling phytoplankton growth rates and chlorophyll to carbon ratios in California coastal and pelagic ecosystems

Qian P. Li,[1] Peter J. S. Franks,[1] Michael R. Landry,[1] Ralf Goericke,[1] and Andrew G. Taylor[1]

Received 7 August 2009; revised 20 April 2010; accepted 4 May 2010; published 5 October 2010.

[1] To understand and quantify plankton community dynamics in the ocean, high-resolution models are needed to capture the temporal and spatial variations of physical, biological, and biogeochemical processes. However, ecosystem models often fail to agree with observations. This failure can be due to inadequacies in the data and/or inadequacies in the model formulation and parameterization. Here we parameterize and optimize a two-phytoplankton functional type model of phytoplankton growth rate and chlorophyll/carbon (Chl:C) ratio using data from the Lagrangian field measurements conducted during process cruises of the Long-Term Ecosystem Research–California Current Ecosystem (CCE) program. We parameterize the model based on a small coastal subset of the data and then extend and test it with the full data set, including data from offshore regions. The CCE process studies were focused on quantifying the size-resolved planktonic growth, grazing, production, and export rates while following water parcels. The resulting data therefore provided strong constraints for the model we employed. The modeled growth rates and Chl:C ratios were in good agreement with observations. Our results indicate that the model can accurately predict Chl:C ratios, biomasses, and growth rates of dominant functional types using relatively easily measured environmental variables (temperature, nutrients, and bulk chlorophyll). The model also accurately reproduces the subsurface maxima of growth rates, the spatial separation of carbon and chlorophyll maxima, and many other observations in the California Current coastal and pelagic ecosystems.

Citation: Li, Q. P., P. J. S. Franks, M. R. Landry, R. Goericke, and A. G. Taylor (2010), Modeling phytoplankton growth rates and chlorophyll to carbon ratios in California coastal and pelagic ecosystems, *J. Geophys. Res.*, *115*, G04003, doi:10.1029/2009JG001111.

1. Introduction

[2] Photosynthesis mediated by unicellular phytoplankton is the base of the entire marine ecosystem and plays a central role in biogeochemical cycling in the oceans [*Falkowski and Raven*, 1999]. The determination of phytoplankton biomass and growth rates or primary productivity has been a central topic in oceanography for many decades [*Behrenfeld et al.*, 2002]. The carbon biomass of phytoplankton is traditionally estimated from cell biovolume by microscopic counting and converted to carbon per cell. Alternatively, biomass can be estimated from measurements of the photosynthetic pigment chlorophyll *a* (Chl), which can be measured continuously, accurately, and even remotely. Conversion between Chl concentration and carbon biomass requires the quantification of chlorophyll *a*/carbon (Chl:C) ratios. However, these vary greatly among species and communities and are affected nonlinearly by ambient nutrient, light, and temperatures [*Geider et al.*, 1997; *Behrenfeld et al.*, 2002; *Wang et al.*, 2009]. Unfortunately, there are very few direct field measurements available to formulate and test current models for Chl:C ratio and phytoplankton growth rates [*Wang et al.*, 2009]. The abilities of ecosystem models to accurately predict phytoplankton growth rates under resource limitation and to accurately predict the Chl:C ratios are therefore two fundamental challenges for understanding the oceanic carbon cycle [*Armstrong*, 2006].

[3] In this paper, we focus on modeling phytoplankton growth rate and Chl:C ratio by combining and modifying the growth model of *Kishi et al.* [2007], the light attenuation and inhibition model of *Platt et al.* [1980], and the *Geider et al.* [1997] Chl:C model. The observed phytoplankton growth rates and Chl:C ratios measured during the Long-Term Ecological Research program (LTER) at the California Current Ecosystem site (CCE) are employed for model formulation and parameterization. Our model was then tested using independent field data. Finally, the model was evaluated using archived environmental data to diagnose the properties of the phytoplankton in a transect across

[1]Scripps Institution of Oceanography, University of California at San Diego, La Jolla, California, USA.

0148-0227/10/2009JG001111

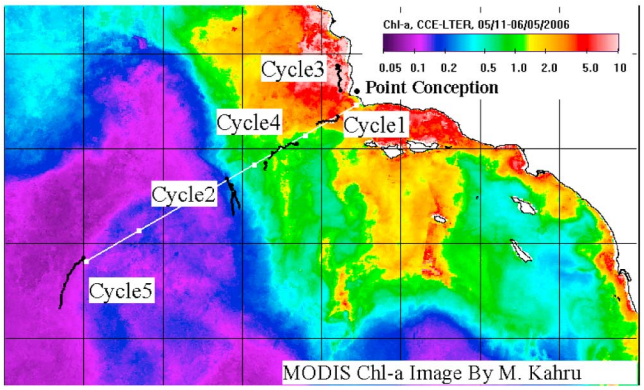

Figure 1. Station map and composite MODIS Chl image of the California Current Ecosystem acquired during CCE Process Cruise P0605 (11 May to 5 June 2006). Small black dots are stations occupied during each cycle; solid white squares and line are a section from CalCOFI line 80.

the CCE. Our results suggest that the model can accurately reproduce many of the biological features observed in the CCE such as growth rates, Chl:C ratios, and phytoplankton community structure.

2. Site Description

[4] The California Current System (CCS) is a southward flowing eastern boundary current, extending between about 49°N and 30°N along the West Coast of the United States. The CCS shows intense mesoscale activity including complex features such as meanders, fronts, and eddies, particularly in its southern regions [*Miller et al.*, 1999]. The rich variety of physical phenomena in this region is a major factor affecting the dynamics and evolution of the local marine ecosystem [*Di Lorenzo et al.*, 2005]. A recent study using 3-D eddy-resolving model simulations with coupled circulation and ecosystem models showed some success in reproducing the large-scale distribution of Chl, nutrients, and phytoplankton biomass in the CCS; however, this model failed to simultaneously represent the detailed biological features of both the eutrophic (inshore) and oligotrophic (offshore) regions [*Gruber et al.*, 2006].

[5] To understand the ecosystem dynamics of the CCS, it is therefore useful to separate the biological or biogeochemical dynamics from their highly complex physical forcings. In this sense, the Lagrangian measurements conducted during the LTER-CCE studies [*Landry et al.*, 2009] are particularly valuable. There were five quasi-Lagrangian experiments conducted during the CCE field cruises in 2006. These experiments were located along the CalCOFI (California Cooperative Oceanic Fisheries Investigations) line 80 (Figure 1), which transited from the coastal upwelling regions to the oligotrophic pelagic ocean. Each experiment was considered as an independent "cycle" (Figure 1: C1 is cycle 1, etc., with five cycles). For each cycle, a suite of measurements was conducted while following a water parcel marked by a satellite-tracked surface drifter drogued at 15 m for a period of 3–5 days [*Landry et al.*, 2009]. The fieldwork included not only biogeochemical measurements (Chl, nutrients, temperature, optical properties, phytoplankton carbon biomass, and others) but also experiments quantifying biological rates (phytoplankton growth rates, zooplankton grazing rates, and particle export rates). These measurements allow for strong constraints of ecosystem models as the horizontal physical perturbations were reduced, and key biological properties and rates were quantified.

3. Methods

3.1. Field Assessments of Phytoplankton Growth Rate

[6] Phytoplankton community growth rates were determined experimentally during CCE Process Cruises P0604 (April 2006) and P0705 (May 2006) using a two-treatment dilution approach as described in the work of *Landry et al.* [2009]. For each cycle, experiments were conducted daily for 3–5 days at 6–8 depths spanning the euphotic zone from 2 to 5 m to the depth corresponding to an average of ~0.4% surface irradiance. Water was collected in predawn CTD casts (0200), and a pair of polycarbonate bottles (2.7 L) was prepared with whole seawater (100%) and 33% whole seawater (diluted with 0.1 μm filtered seawater) for each depth. The bottles were then tightly capped, placed into net bags, and clipped onto attached rings at the depth of collection onto at tether line under the surface drifter. Incubations were done under in situ conditions of light and temperature for 24 h.

[7] Rate estimates were based on initial and final subsamples (250 mL) taken for fluorometric analyses of Chl. Instantaneous rates of phytoplankton growth (μ, d^{-1}) were computed as $\mu = \eta + (\eta_d - \eta)/(1 - 0.33)$, where $\eta = [\ln(Chl_t/Chl_0)]/\Delta t$ and $\eta_d = [\ln(Chl_t^d/Chl_0^d)]/\Delta t$ are the calculated rates of change of Chl in the natural and diluted treatments (assuming constant exponential growth and mortality) and the factor 0.33 is the fraction of raw seawater in the diluted sample. Chl_0 and Chl_0^d are the initial Chl concentrations in the raw and diluted samples, and Chl_t and Chl_t^d are the Chl concentrations after an incubation of time Δt [*Landry et al.*, 2009].

3.2. Field Determination of Phytoplankton Chlorophyll and Carbon Biomass

[8] For each experimental cycle, water samples for Chl analyses and carbon biomass assessments of phytoplankton were collected daily close to the drift array on the same hydrocast (0200 CTD) and at the same depths at which growth rate experiments were initiated. Samples were immediately filtered onto GF/F filters, and the Chl was extracted with 90% acetone in a dark refrigerator for 24 h. Extracted samples were shaken, centrifuged, and quantified on a calibrated Turner Designs model 10 fluorometer. Phytoplankton carbon biomass was determined from a combination of flow cytometry (FCM) for photosynthetic prokaryotes and epifluorescence microscopy (EPI) for autotrophic eukaryotes. Phytoplankton Chl:C ratios were determined for each day and depth of collection by dividing the extracted community estimate of Chl by the corresponding total community carbon of all Chl-containing populations determined by FCM and EPI.

[9] FCM samples (2 mL) were preserved with 0.5% paraformaldehyde, frozen in liquid nitrogen, and stored at −80°C. Thawed samples were analyzed using a Beckman-Coulter EPICS Altra flow cytometer with dual lasers (1 W at

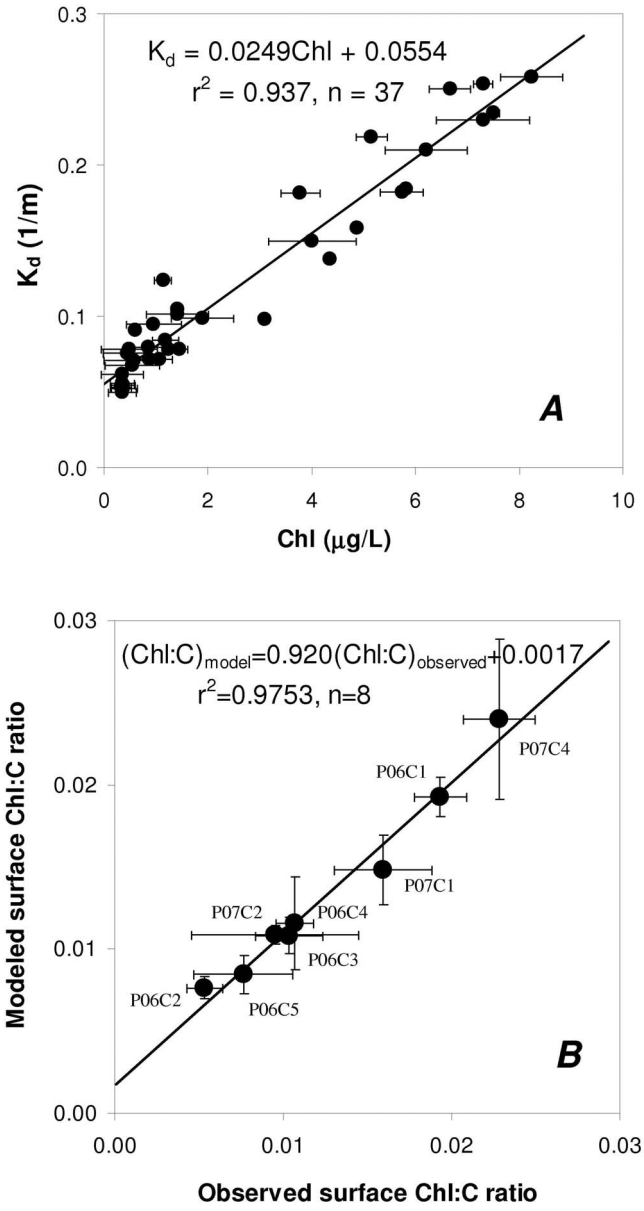

Figure 2. (a) Relationship of K_d and Chl in the CCE. (b) Comparison of observed and modeled Chl:C ratios (NSG model) in the surface water of CCE. Data are from CCE Process Cruises P0605 and P0704; data labels give cruise year and cycle number. Error bars are standard deviations.

488 nm, 200 mW in UV) and a syringe pump for volumetric sample delivery. *Prochlorococcus* and *Synechococcus* abundances were converted to biomass estimates using factors of 32 and 100 fg C cell^{-1}, respectively [*Garrison et al.*, 2000]. EPI samples were analysed on slides in two size classes. Cells <10 μm were enumerated in 50 mL aliquots preserved with paraformaldehyde (0.5% final concentration), stained with proflavin (0.33% wt/vol), and DAPI (10 μg mL^{-1}) and mounted onto black 0.8 μm black Nuclepore filters. Larger cells were enumerated from 300 to 500 mL subsamples, preserved according to the work of *Sherr and Sherr* [1993], stained with proflavin and DAPI, and mounted onto 8 μm black Nuclepore filters. The slides were imaged and digitized at 630× (50 mL) or 200× (500 mL) using a Zeiss AxioVert 200M microscope with an AxioCam HR color CCD digital camera. Cell biovolumes (BV; μm^3) were determined from size measurements using the formula for a prolate sphere. Carbon biomass was computed from biovolumes based on equations from the work of *Eppley et al.* [1970] for diatoms ($\log_{10}$C = 0.76($\log_{10}$BV) − 0.352) and nondiatom phytoplankton ($\log_{10}$C = 0.94($\log_{10}$BV) − 0.60).

3.3. Model of Phytoplankton Growth Rate

[10] Our goal is to formulate a model of phytoplankton growth rate as a function of variations in light, nutrients, and temperature. We include two types of phytoplankton: diatoms (which require silicon) and nondiatoms (including dinoflagellates, cyanobacteria, etc.). The dependence of phytoplankton growth rate μ (units: d^{-1}) on nutrients, temperature, and light can be expressed as

$$\mu = V_m^0 \varphi(\mathrm{N}, \mathrm{Si}) \xi(T) \gamma(\mathrm{PAR}), \quad (1)$$

where V_m^0 is the maximum growth rate of phytoplankton at a reference temperature (0°C) without nutrient limitation or light limitation. φ, ξ, and γ are functions representing the growth response to variations in nutrient, temperature, and light, respectively. A variety of formulae for each of these functions (φ, ξ, and γ) can be found in the literature and have been reviewed recently by *Tian* [2006]. The model formulae and parameterizations used in this study were selected based on their ability to reproduce the field data.

[11] While there are many temperature and nutrient functions to be found in the literature [e.g., *Franks et al.*, 1986; *Moisan and Hofmann*, 1996; *Geider et al.*, 1997; *Chai et al.*, 2002; *Follows et al.*, 2006; *Kishi et al.*, 2007; *Wang et al.*, 2009], we base our model on the NEMURO model of *Kishi et al.* [2007]. Below, we describe our changes to the phytoplankton growth model of *Kishi et al.* [2007]. These changes were mainly to the parameterization of the light response and the inclusion of a model for the Chl:C ratio.

3.3.1. Light Attenuation

[12] The vertical distribution of photosynthetically active radiation (PAR; units: μEinstein m^{-2} s^{-1}) with depth z is

$$\mathrm{PAR}(z) = \mathrm{PAR}(0) \exp\left(-\int_0^z K_d dz\right), \quad (2)$$

where PAR(0) is the surface PAR and K_d is the diffuse attenuation coefficient (units: m^{-1}). K_d is a function of attenuation due to seawater (K_{sw}) and the attenuation due to phytoplankton ($K_{ph\text{-}chl}$),

$$K_d = K_{sw} + K_{ph-chl}(\mathrm{Chl}). \quad (3)$$

From field data (Figure 2a), we find K_{sw} = 0.0554 m^{-1} and $K_{ph\text{-}chl}$ = 0.0249 (μg Chl L^{-1})$^{-1}$ m^{-1} (Table 1). K_d was obtained from the vertical gradient of PAR measured by the PAR sensor on the CTD/rosette system. PAR for all the selected casts was normalized to PAR at noon. When no measurements were available, PAR was estimated from equation (2) using a daily PAR(0) of 708.4 μEinstein m^{-2} s^{-1} for clear skies during May 2006.

Table 1. List of Parameters and Terms

Symbol	Definition	Nondiatom	Diatom	Unit	Source
α	initial slope of P-E curve	0.0030	0.0061	(μEinstein m^{-2} s^{-1} $d)^{-1}$	data
α^{chl}	chlorophyll specific initial slope of P-E curve	0.28 ± 0.11	0.28 ± 0.11	(mg C mg Chl^{-1}) (μEinstein m^{-2} s^{-1} $d)^{-1}$	data
β	photoinhibition coefficient	0.0017	0.0002	(μEinstein m^{-2} s^{-1} $d)^{-1}$	data
ψ	ammonium inhibition of nitrate uptake	1.5	4.6	(μmol $L^{-1})^{-1}$	*Kishi et al.* [2007]
$(Chl:C)_{min}$	minimum Chl:C ratio	0.000	0.005	mg Chl mg C^{-1}	data
$(Chl:C)_{max}$	maximum Chl:C ratio	0.030	0.065	mg Chl mg C^{-1}	data
k_T	temperature coefficient of growth	0.0693	0.0693	$(°C)^{-1}$	*Kishi et al.* [2007]
K_{NO3}	half-saturation constant for NO_3 uptake	1.0	3.0	μmol L^{-1}	*Kishi et al.* [2007]
K_{NH4}	half-saturation constant for NH_4 uptake	0.1	0.3	μmol L^{-1}	*Kishi et al.* [2007]
K_{Si}	half-saturation constant for Si uptake	4.0	4.0	μmol L^{-1}	*Kishi et al.* [2007]
K_{sw}	diffuse attenuation due to seawater	0.0554	0.0554	$(m)^{-1}$	data
$K_{ph\text{-}chl}$	diffuse attenuation due to Chl *a*	0.0249	0.0249	$(m)^{-1}(\mu g\ Chl\ L^{-1})^{-1}$	data
K_d	diffuse attenuation coefficient	not a constant	not a constant	$(m)^{-1}$	
P_m^C	C-specific maximum photosynthetic rate	not a constant	not a constant	$(d)^{-1}$	
V_m^0	maximum growth rate at 0°C	0.4	1.0	$(d)^{-1}$	data
V_s^{chl}	Chl *a*-specific light saturated growth rate	36.72 ± 19.20	36.72 ± 19.20	(mg C mg Chl^{-1}) $(d)^{-1}$	data

3.3.2. Light-Limited Growth

[13] A common approach to modeling the response of phytoplankton photosynthetic rate to irradiance is to construct photosynthesis-irradiance (P-I or, more recently, P-E) response curves, which can include photoinhibition [e.g., *Platt et al.*, 1980]. Following this approach, the growth response to changes in PAR can be expressed as

$$\gamma(\mathrm{PAR}) = [1 - \exp(-\alpha \mathrm{PAR}/V_m^0)]\exp(-\beta \mathrm{PAR}/V_m^0), \quad (4)$$

where α is the initial slope of P-E curve [units: (μEinstein m^{-2} s^{-1} $d)^{-1}$] and β is the photoinhibition parameter [units: (μEinstein m^{-2} s^{-1} $d)^{-1}$]. V_m^0, the maximum specific growth rate [units: d^{-1}] under light saturation without photoinhibition, is assumed equal to the maximum specific light-saturated photosynthetic rate.

[14] Substituting equation (4) into equation (1), we have

$$\mu = V_m^0 \varphi(\mathrm{N,Si})\xi(\mathrm{T})[1 - \exp(-\alpha \mathrm{PAR}/V_m^0)]\exp(-\beta \mathrm{PAR}/V_m^0). \quad (5)$$

Field measurements were made of the Chl-normalized photosynthetic parameter α^{chl} and the Chl-normalized light-saturated maximum photosynthetic rate V_s^{chl} (both were measured at in situ temperature and normalized to 0°C by dividing them by a temperature-dependent factor of exp ($k_T T$), where k_T = 0.0693°C^{-1}, and under nutrient-rich conditions). The relationship between α and α^{chl} is

$$\alpha = \alpha^{chl}\mathrm{Chl{:}C}. \quad (6)$$

Measurements made during the CCE study give α^{chl} = 0.28 ± 0.11 (mg C/mg Chl) (μEinstein m^{-2} s^{-1} $d)^{-1}$ and V_s^{chl} = 36.7 ± 19.2 (mg C/mg Chl) d^{-1} (Table 1). These rates were not much different from those in the lower euphotic zone off Baja California [*Valdez-Holguin et al.*, 1998]. The observed surface Chl:C ratio was ~0.010 mg Chl/mg C in the pelagic region (dinoflagellate dominated) and ~0.021 mg Chl/mg C in the coastal region (diatom dominated). Thus, we estimated α to be ~0.0030 (μEinstein m^{-2} s^{-1} $d)^{-1}$ for nondiatoms and ~0.0061 (μEinstein m^{-2} s^{-1} $d)^{-1}$ for diatoms (Table 1). Estimates of V_m^0 (equal to V_s^{chl}Chl:C) were 0.37 ± 0.20 d^{-1} in pelagic regions and 1.03 ± 0.53 d^{-1} in coastal regions. In the model, we set V_m^0 to be ~0.4 d^{-1} for nondiatom phytoplankton (mainly dinoflagellates) and ~1.0 d^{-1} for diatoms (Table 1). These values were also in good agreement with those observed by *Goericke* [2002]. To estimate the light inhibition parameter β for diatom and nondiatom phytoplankton, we used field measurements of temperature, nutrients, light, and the observed nondiatom/diatom ratio from cycle 1 and equation (5). The values of β were then chosen to minimize the sum of the squared residuals of the modeled and observed growth rates of cycle 1. This approach gave values of β of 0.0017 (μEinstein m^{-2} s^{-1} $d)^{-1}$ for nondiatom phytoplankton and 0.0002 (μEinstein m^{-2} s^{-1} $d)^{-1}$ for the diatoms (Table 1).

3.3.3. Temperature Response $\xi(T)$

[15] The growth response to temperature is commonly modeled as an exponential function [e.g., *Eppley*, 1972; *Kishi et al.*, 2007],

$$\xi(T) = \exp(k_T T), \quad (7)$$

where T is in °C and k_T is the temperature-dependence coefficient (units: °C^{-1}, Table 1).

3.3.4. Nitrogen Limitation f(N)

[16] Two forms of dissolved nitrogen were included in the model: nitrate (NO_3) and ammonium (NH_4). Nitrate uptake follows Michaelis-Menten kinetics with a factor representing the effect of ammonium inhibition on nitrate uptake [*Kishi et al.*, 2007],

$$f(\mathrm{N}) = \frac{\mathrm{NO_3}}{\mathrm{NO_3} + K_{NO3}}\exp(-\psi \mathrm{NH_4}) + \frac{\mathrm{NH_4}}{\mathrm{NH_4} + K_{NH4}}, \quad (8)$$

where K_{NO3} is the half saturation constant of nitrate uptake, ψ is the ammonium inhibition parameter, and K_{NH4} is the half saturation constant for ammonium uptake (see Table 1 for values).

3.3.5. Silicon Limitation g(Si)

[17] Diatoms are distinguished by their requirement of silicon for their frustule. Silicon limitation of diatom growth is often modeled as

$$g(\mathrm{Si}) = \frac{\mathrm{Si(OH)_4}}{\mathrm{Si(OH)_4} + K_{Si}}, \quad (9)$$

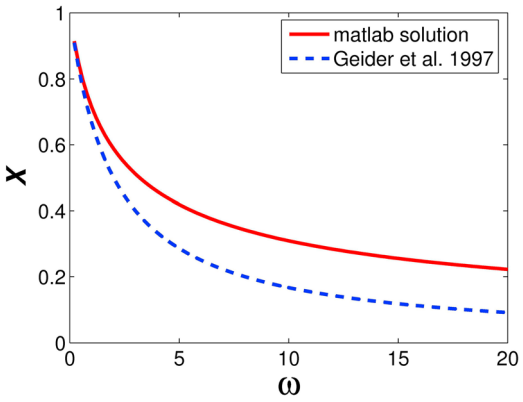

Figure 3. Calculating the Chl:C ratio: relationship of X and ω. Dashed line is the analytical approximation to the model of *Geider et al.* [1997] (equation (15)), and red line is the numerical solution to equation (14) (the NSG model). See text for details.

where K_{Si} is the half saturation constant for silicon uptake (Table 1) [*Chai et al.*, 2002; *Kishi et al.*, 2007]. We use this formulation for our model.

3.3.6. Nitrogen and Silicon Colimitation φ(N, Si)

[18] In the model, colimitation by nitrogen and silicon of diatom growth was expressed as the minimum of the functions describing the single-nutrient limitation [*Moisan and Hofmann*, 1996; *Chai et al.*, 2002; *Kishi et al.*, 2007],

$$\varphi(\mathrm{N},\mathrm{Si}) = \min\{f(\mathrm{N}), g(\mathrm{Si})\}. \tag{10}$$

3.4. Modeling the Chl:C ratio

[19] Several models for phytoplankton Chl:C ratio have been developed, including empirical models based on experiments [*Cloern et al.*, 1995; *Wang et al.*, 2009] and theoretical models based on phytoplankton physiology [*Geider et al.*, 1997; *Armstrong*, 2006]. We begin with the *Geider et al.* [1997] model (hereafter referred to as G97) describing phytoplankton Chl:C under balanced growth, which provides a dynamic description of photoacclimation under nutrient-saturated conditions at constant temperature. Here equation (A10) of G97 was rearranged to

$$(\mathrm{Chl{:}C})^2 = ka\left[1 - \exp\left(-\frac{\mathrm{Chl{:}C}}{a}\right)\right], \tag{11}$$

where $a = \frac{P_m^C}{\alpha^{chl}\mathrm{PAR}}$. P_m^C is the maximum carbon-specific photosynthetic rate at constant temperature without light limitation. k is the maximum Chl:C ratio (in the sense of G97) of phytoplankton grown in the dark under nutrient-saturated conditions and constant temperature. *Armstrong* [2006] analyzed a modified form of G97 [*Geider et al.*, 1998] both of which incorporate variable internal nutrient stores in the phytoplankton. This allowed for changing N:C ratios in the cells. Our model for the Chl:C ratio (equation (11)) is identical to the *Armstrong* [2006] model (his equation (A.5)) if a constant N:C ratio is used (the Redfield ratio).

Let

$$X = \frac{\mathrm{Chl{:}C}}{k} \tag{12}$$

and

$$\omega = \frac{k\alpha^{chl}}{P_m^C}\mathrm{PAR}. \tag{13}$$

Substituting equations (12) and (13) into equation (11) yields

$$X^2 = \frac{1 - \exp(-\omega X)}{\omega}. \tag{14}$$

The above equation is transcendental and cannot be solved directly for X. G97 derived an approximate solution to this,

$$X = \frac{1}{1 + 0.5\omega}. \tag{15}$$

We solved the nonlinear equation numerically using *fminsearch* of Matlab and compared it with the G97 approximation. To distinguish our numerically solved model from the analytical approximation of G97, we refer to our Chl:C model as the "NSG" model (Numerical Solution to Geider model). Our results suggest that the G97 approximation significantly underestimates X as ω increases (Figure 3).

3.4.1. Relationship of Chl:C and Growth Rate

[20] To compute the Chl:C, the maximum carbon specific light-saturated photosynthetic rate P_m^C is required (see equation (11)). We include nutrient, temperature and photoinhibition effects on P_m^C and assume constant C:N and C:Si ratios. Solving equation (5) when $d\mu/d\mathrm{PAR} = 0$, similar to *Harrison and Platt* [1986], we obtain

$$P_m^C = V_m^0 \xi(T)\varphi(\mathrm{N},\mathrm{Si})[\alpha/(\alpha+\beta)][\beta/(\alpha+\beta)]^{\beta/\alpha}. \tag{16}$$

Using the above equation and solving equation (14) numerically (see Figure 3), we obtain a value for X. The Chl:C ratio of the phytoplankton is then calculated as

$$\mathrm{Chl{:}C} = X(\mathrm{Chl{:}C})_{max}, \tag{17}$$

with the constraint that $\frac{(\mathrm{Chl{:}C})_{min}}{(\mathrm{Chl{:}C})_{max}} < X < 1$, where $(\mathrm{Chl{:}C})_{min}$ is the minimum and $(\mathrm{Chl{:}C})_{max}$ is the maximum Chl:C ratio (Table 1).

3.4.2. Parameterization of the Chl:C Model

[21] We used the field data of Chl:C ratios measured at the sea surface to parameterize the Chl:C ratio models for diatoms and nondiatoms. For our NSG model, we estimated $(\mathrm{Chl{:}C})_{max}$ to be 0.030 g Chl/g C for nondiatoms and 0.065 g Chl/g C for diatom. $(\mathrm{Chl{:}C})_{min}$ was found to be 0 g Chl/g C for nondiatoms and 0.005 g Chl/g C for diatoms (Table 1). For G97 model, $(\mathrm{Chl{:}C})_{max}$ was 0.060 g Chl/g C for nondiatoms and 0.075 g Chl/g C for diatoms, while $(\mathrm{Chl{:}C})_{min}$ was 0.003 g Chl/g C for nondiatoms and 0.005 g Chl/g C for diatoms. In the model, the phytoplankton communities in coastal and pelagic oceans vary due to the relative proportions of diatoms and nondiatoms. At the offshore stations, where diatom concentrations were extremely low, the observed community Chl:C ratios were mostly equal to the Chl:C ratios of the nondiatom phytoplankton. These data were then used to quantify the minimum and maximum Chl:C ratios for the nondiatom phytoplankton. Our approach is simply based on linear regression of Chl:C ratios with X, calculated from the model. The slope is $(\mathrm{Chl{:}C})_{max}$ and the minimum X obtained is the ratio of $(\mathrm{Chl{:}C})_{min}$ over

Table 2. Mean Biogeochemical and Growth Rate Data of Five Cycles During May 2006

	Depth (m)	T (°C)	NO_3 (μmol L^{-1})	NH_4 (μmol L^{-1})	$SiOH_4$ (μmol L^{-1})	Chl (μg L^{-1})	PAR (%)	Diatom (%)	Biomass (μg C L^{-1})	Chl:C	μ (d^{-1})
Cycle1	2.9	12.21	8.59	0.49	11.16	6.02	59.15	0.19	295.7	0.020	0.44
	5.9	12.18	8.70	0.62	11.40	6.18	34.34	0.21	223.5	0.028	0.57
	8.8	12.08	8.87	0.53	11.37	6.10	20.35	0.26	168.0	0.036	0.48
	12.9	12.02	9.10	0.54	11.60	6.48	9.63	0.23	216.5	0.030	0.57
	19.8	11.91	9.57	0.74	12.08	6.03	2.74	0.21	233.6	0.026	0.24
	25.7	11.71	10.85	0.70	13.27	5.11	0.95	0.29	172.9	0.030	0.22
	35.8	11.24	12.92	0.81	15.03	3.16	0.15	0.30	75.9	0.042	−0.05
	50.6	10.30	19.30	0.42	20.52	0.81	0.01	0.08	15.6	0.052	
Cycle2	5.9	14.57	0.12	0.25	1.64	0.13	72.93	0.00	16.7	0.008	0.29
	12.9	14.48	0.11	0.15	1.73	0.13	50.37	0.01	22.1	0.006	0.49
	21.1	14.39	0.17	0.23	1.68	0.14	32.70	0.00	26.8	0.005	0.34
	40.8	14.00	0.12	0.19	1.64	0.23	11.44	0.00	16.7	0.014	0.48
	60.6	13.82	0.14	0.23	1.75	0.44	4.00	0.01	26.1	0.017	0.10
	70.8	13.60	0.40	0.36	2.02	0.69	2.33	0.01	41.2	0.017	0.07
	80.9	13.37	2.15	0.28	3.07	0.66	1.36	0.02	22.8	0.029	0.01
	100.7	12.06	6.47	0.31	5.90	0.40	0.48	0.03	10.0	0.040	0.03
Cycle3	3.1	13.51	1.73	0.49	6.75	6.69	52.95	0.15	325.1	0.021	0.14
	5.9	13.43	1.87	0.42	6.89	6.99	29.76	0.12	492.5	0.014	0.44
	9.0	13.19	2.62	0.60	8.16	6.43	15.61	0.16	461.9	0.014	0.39
	13.2	12.81	5.52	0.71	10.82	4.55	6.58	0.10	226.4	0.020	0.32
	20.2	12.51	7.30	0.75	11.80	4.13	1.56	0.12	243.2	0.017	0.19
	26.3	11.96	10.30	0.84	13.71	2.96	0.45	0.19	159.1	0.019	0.32
Cycle4	3.4	14.72	0.99	0.29	3.18	1.10	76.48	0.07	66.1	0.017	0.40
	8.6	14.73	1.04	0.37	3.27	1.13	50.90	0.07	65.7	0.017	0.53
	12.8	14.73	1.04	0.26	3.27	1.08	36.27	0.05	58.4	0.019	0.45
	19.5	14.73	1.06	0.39	3.25	1.08	21.65	0.07	65.6	0.017	0.62
	25.1	14.74	1.06	0.39	3.29	1.08	13.67	0.08	65.3	0.016	0.59
	31.2	14.71	1.11	0.30	3.32	1.11	8.23	0.07	60.4	0.018	0.58
	41.2	13.48	5.05	0.53	6.10	1.50	3.71	0.14	64.4	0.023	0.10
	51.1	11.26	14.10	0.36	13.41	0.98	1.67	0.09	44.0	0.022	0.06
Cycle5	3.1	16.38	0.28	0.27	1.90	0.11	80.26	0.00	9.2	0.012	0.13
	13.3	16.35	0.22	0.23	1.84	0.11	39.13	0.02	8.9	0.012	0.30
	21.4	16.27	0.23	0.19	1.87	0.11	22.11	0.02	6.3	0.018	0.37
	31.2	15.87	0.24	0.27	1.70	0.12	11.03	0.01	6.5	0.019	0.32
	51.2	15.00	0.24	0.19	2.01	0.32	2.67	0.01	16.7	0.019	0.03
	61.0	14.18	0.27	0.17	2.53	0.73	1.34	0.01	34.7	0.021	0.15
	70.6	13.30	1.87	0.23	3.51	1.22	0.68	0.02	43.3	0.028	0.00
	90.0	12.52	6.01	0.27	5.75	1.08	0.26	0.02	40.8	0.027	−0.03

$(Chl:C)_{max}$. Using the $(Chl:C)_{max}$ and $(Chl:C)_{min}$ values of nondiatoms found in the offshore regions, together with the observed percentage of diatoms in the total phytoplankton biomass and the observed community Chl:C ratios in coastal regions, we could determine $(Chl:C)_{max}$ and $(Chl:C)_{min}$ for the diatoms.

4. Results and Discussion

4.1. Comparison of Modeled and Observed Growth Rates

[22] In situ measurements of nutrients, light, and temperature (mean values were shown in Table 2) were used to compute the growth rates for the two phytoplankton functional groups (diatoms μ_d and nondiatoms μ_n) in the model for each of the five sampling cycles (Figure 4). Cycles were grouped by location (see Figure 1): coast (cycle 1 and cycle 3), transition zone (cycle 4), and open ocean (cycle 2 and cycle 5). Our model was able to capture the patterns in growth rate among these cycles: growth rate was high near the coast with a strong vertical gradient; relatively low growth rates were predicted in the open ocean, with weaker vertical gradients (Figure 4).

[23] Cycles 1 and 3 captured a relatively recent upwelling event, showing high concentrations of nutrients and Chl, in contrast to the offshore stations of cycles 2 and 5, which had low surface Chl and deep nutriclines [*Landry et al.*, 2009]. Cycle 4 represented a transitional region between the upwelling system and the offshore oligotrophic waters [*Landry et al.*, 2009]. Both diatoms and nondiatoms showed significantly higher growth rates in the coastal regions (cycles 1 and 3) than offshore; however, these populations were subject to strong light limitation below the surface. In contrast, phytoplankton in the oligotrophic regions (cycles 2 and 5) grew much more slowly, largely due to nutrient (N and Si) limitation.

[24] The community growth rate (μ) in the model was calculated as the sum of the carbon biomass-weighted growth rates of each functional group (μ_d or μ_n). Excepting the surface layer of cycle 2, the modeled μ agrees well with the observed μ for both coastal and offshore regions (r^2 = 0.5916, n = 37, $p < 0.0001$, Figure 4). This agreement between model and observation suggests that our model accurately diagnoses the growth rates of phytoplankton in the CCE where diverse physical and chemical forcings create a very complex and dynamic system. In cycle 2, the modeled μ is much lower than the observed μ in the surface. One explanation for this discrepancy may be the utilization of dissolved organic nitrogen or phagotrophy of smaller prey by mixotrophic nondiatom phytoplankton when the

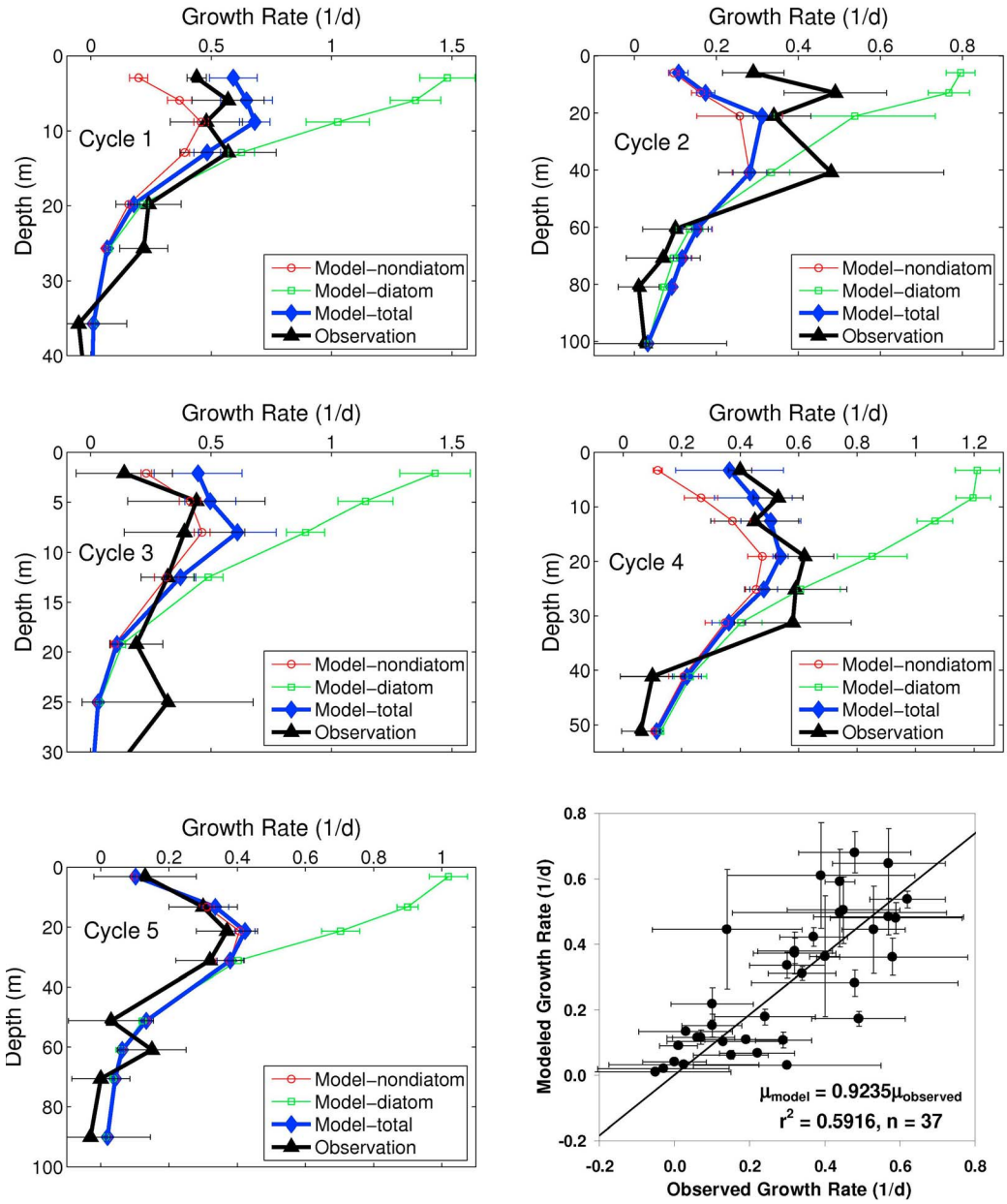

Figure 4. Vertical distribution of observed and modeled growth rates for CCE Process Cruise P0605, cycles 1–5. The last frame is the comparison between model and data. Open squares show the growth rates of diatoms, and open circles show the growth rates of nondiatom phytoplankton. Growth rates were measured at multiple stations during a cycle and are plotted as the mean and standard deviation over the cycle. CTD and nutrient data from the same stations were used to calculate the model growth rates, which are also plotted as mean and standard deviation for the cycle.

ambient inorganic nitrogen is sparse. These processes are not included in our model. Diatom abundances are low in both cycles 2 and 5, and the community is dominated by nondiatom small phytoplankton, which are typical in the oligotrophic ocean. Compared to cycle 2, both μ_d and μ_n in cycle 5 were slightly higher in the upper euphotic zone but much lower than those found in the coastal stations (cycles 1 and 3).

[25] Both model and observations suggested a subsurface maximum of community growth rate in all five cycles. For coastal upwelling regions such as cycles 1 and 3, the maximum growth rate was located at about 10–20 m depth, while it was found between 10 and 30 m in the transitional zone of cycle 4 and 20–40 m in the offshore stations of cycles 2 and 5. In addition to environmental regulation of growth rate, our model suggests that community structure plays an important role in determining the vertical pattern of phytoplankton growth rates through the water column. Because of different light inhibition responses, individual phytoplankton types have different growth rate profiles (Figure 4). Generally, nondiatom phytoplanktons were strongly affected by light inhibition at the surface, with

maximum growth rates located at the subsurface. Diatoms, however, showed maximal rates of growth at the surface, decreasing with depth. In coastal regions, the community growth rate had contributions from both diatom and nondiatom phytoplankton and was relatively homogenous through the upper euphotic zone. In offshore regions where diatoms were less abundant, the community growth rate was mostly controlled by nondiatom phytoplankton and showed substantial subsurface maxima.

[26] *Landry et al.* [2009] speculated that the subsurface maximum of growth rate could be attributed to a new iron source associated with the nitracline relieving the stress of iron limitation on diatoms. Iron limitation of diatom growth in the coastal California upwelling system was reported previously [*Hutchins and Bruland*, 1998; *King and Barbeau*, 2007], where unused nitrate in the surface could lead to high-nutrient low-chlorophyll (HNLC) conditions. However, iron limitation of diatom growth has only been found in limited areas of the transitional zone of the CCE [*King and Barbeau*, 2007]. If iron limitation were a general feature of the CCE, we would expect to see much higher community growth rates from our model than from the field measurements since our model does not include iron limitation of growth and is parameterized with the data from coastal regions where iron is rich. Instead, our model suggests that the subsurface growth-rate maximum is a consequence of the changing phytoplankton community structure across the CCS. This, however, does not contradict the recent hypothesis of nitrogen-limited phytoplankton biomass but iron-limited diatom growth rate in this region [*King and Barbeau*, 2007]: the abundance of diatoms is very low in offshore regions and contributes very little to the total community growth rate. Diatoms thus do not contribute significantly to our model-data comparisons in the offshore regions where iron input is low. Future development of CCE models may benefit from adding iron as a component of nutrient colimitation to fully resolve the small-scale patterns of growth rate in this complex ecosystem.

4.2. Comparison of Modeled and Observed Chl:C Ratio

[27] A comparison between modeled (NSG model) and observed Chl:C ratios at the sea surface (Figure 2b) shows that the model has considerable skill in reproducing the patterns in Chl:C ($r^2 = 0.9753$, $n = 8$, $p < 0.0001$). There was a general trend of higher Chl:C ratios at the surface of coastal regions (>0.02 g Chl/g C) than offshore regions (<0.01 g Chl/g C).

[28] The vertical distributions of Chl:C for nondiatom phytoplankton and diatoms can be predicted from the model for each sampling cycle. In addition, the total community Chl:C ratio was computed by multiplying the observed percentage (based on carbon) of each phytoplankton type by its individual Chl:C ratio. We also examined the overall performance of the "original" G97 model (analytical approximation) [*Geider et al.*, 1997] using the CCE field hydrographic data and compared these results with those of the NSG model (G97 solved numerically) as well as the field measurements. The data set and approach to parameterize the G97 model were exactly the same as those employed for the NSG model. The results suggested that our parameterized NSG model was in good agreement with the field observations, but the original G97 model significantly overestimated the Chl:C ratio at depth (Figure 5). As mentioned above (also Figure 3), the original G97 approximation leads to an underestimate of Chl:C at the sea surface where light levels are high (i.e., a larger ω in equation (13)). Carbon fixation thus may be underestimated in low-light high-chlorophyll regions of the water column when the original G97 approximation is used to estimate oceanic primary production.

[29] At the sea surface, the Chl:C ratio of phytoplankton (Table 2 and Figure 5) was low due to the strong light intensity compared to deeper layers. Chl:C increased with depth, presumably to enhance the efficiency of light harvesting at depth and in response to nutrient inputs from below (in offshore stations where nutrients were limiting). Near the bottom of euphotic zone, lower temperatures offset the effects of light and nutrients, giving a relatively constant Chl:C ratio. These findings were consistent with those from a large-scale 3-D model simulation conducted in the equatorial Pacific Ocean, which showed complex effects of light, nutrients, and temperature in regulating the phytoplankton Chl:C ratio [*Wang et al.*, 2009]. Besides nutrients, light, and temperature, our model suggests that the community structure is an important determinant of the bulk community Chl:C and may influence the amount of organic carbon that could be exported to the deep ocean via the "biological pump."

[30] Our model suggests that the community Chl:C ratio is strongly determined by the phytoplankton composition, specifically the percentage of diatoms in the community. Some field observations [*Veldhuis and Kraay*, 2004; *Llewellyn et al.*, 2005] have indicated lower Chl:C ratios for small phytoplankton than for diatoms. Similarly, recent investigations in a subtropical estuary showed evidence that lower phytoplankton Chl:C ratios corresponded to a higher percentage of phytoplankton <5 μm [*Putland and Iverson*, 2007]. Our model supports these findings: nondiatoms showed lower Chl:C ratios than diatoms under constant nutrients, light, and temperature (results not shown). This was partly due to higher rates of diatom growth, which will lead to lower ω (equation (13)) and thus higher X (see Figure 3). We also found that the $(\mathrm{Chl:C})_{\max}$ for diatoms was much higher than that of nondiatom phytoplankton, which may suggest that diatoms could potentially use a larger fraction of photosynthetic output for chlorophyll synthesis.

4.3. Patterns of Growth Rate and Chl:C Ratio in the Southern California Current Ecosystem

[31] Our newly parameterized model can now be evaluated using easily measured environmental variables (temperature, nutrient concentrations, and Chl) in order to diagnose vertical profiles of the bulk community growth rates and Chl:C ratios, as well as the growth rates and Chl:C ratios of the diatoms and nondiatoms. Here we apply the model to CalCOFI data to hindcast these properties. In order to predict the growth rate and the Chl:C ratio of the phytoplankton community, we need to know the ratio of nondiatom/diatom ($R_{\mathrm{n:d}}$) in terms of carbon in the phytoplankton community. Since there is no general model

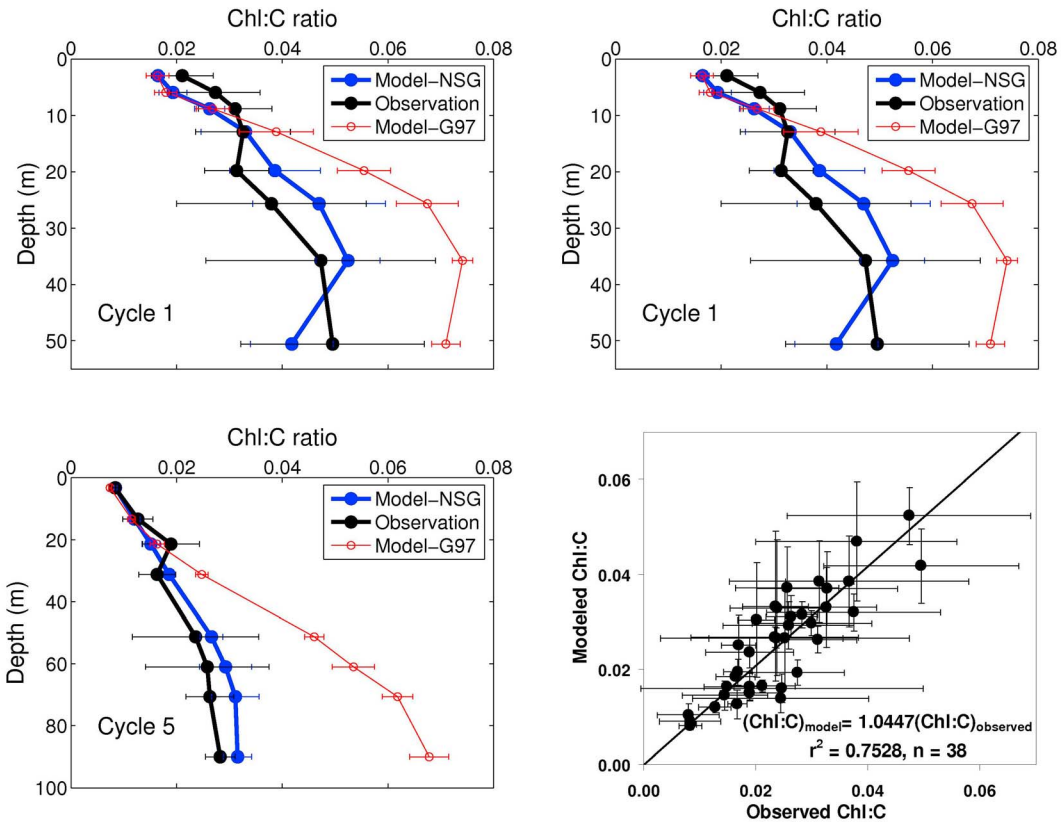

Figure 5. Vertical distribution of Chl:C ratio from observations, G97 [*Geider et al.*, 1997] model, and the NSG model for CCE Process Cruise P0605, cycles 1, 2, and 5. The last frame shows the comparison between the observation and our NSG model. Error bars are standard deviations of Chl:C ratio estimates from measurements and from models for each cycle.

for phytoplankton community structure, we therefore estimated $R_{n:d}$ from CCE field data, deriving an empirical relationship between $R_{n:d}$ and total Chl (Figure 6). The ratio of nondiatom to diatom was fit by the power law relationship $R_{n:d} = 24.49\text{Chl}^{-1.0229}$. The fraction of diatom biomass to the total phytoplankton biomass was then calculated by $1/(R_{n:d} + 1)$. Now knowing the temperature, Chl concentration, and nutrient concentrations (all easily measured at sea), we can compute vertical profiles of the growth rates and Chl:C ratios of the two phytoplankton types, as well as the bulk community growth rates and Chl:C ratios.

[32] Here we use data from CalCOFI line 80.0, cruise 0604 in the southern CCE (Figure 7), conducted during April 2006 and located near CCE cruise 0605 (with which we parameterized our model), but 1 month earlier than the CCE study. During the CalCOFI transect (Figure 7), coastal upwelling had created strong seasonal thermocline and nutriclines that deepened with distance away from the shore. The depth of the deep Chl maximum (DCM) varied from near the surface onshore to ~75 m offshore following the 13.5°C isotherm. The model predicted that the strongest vertical gradient of Chl:C ratio was near the DCM. The modeled community growth rate (μ) and diatom growth rate (μ_d), however, showed different spatial patterns with the combined effects from nutrients, temperature, light, and Chl (Figure 7): the diatom growth rate tended to decrease

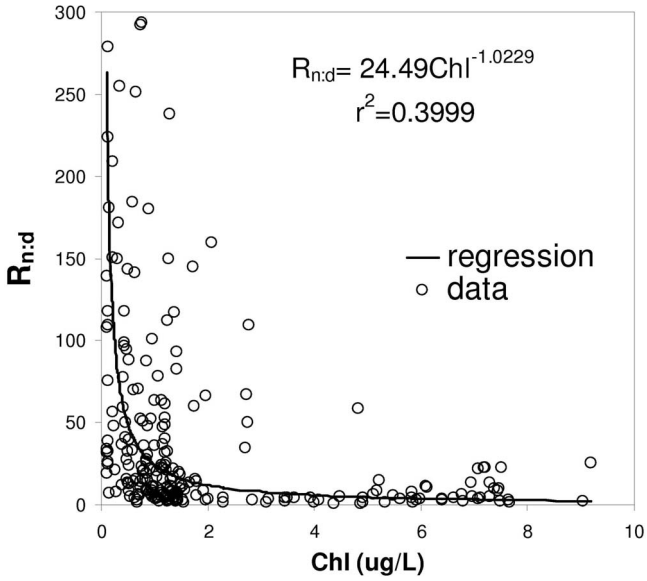

Figure 6. Relationship of nondiatom/diatom ratio versus total Chl in the CCE Process Cruises P0605 and P0704. The regression line was calculated from log-transformed data.

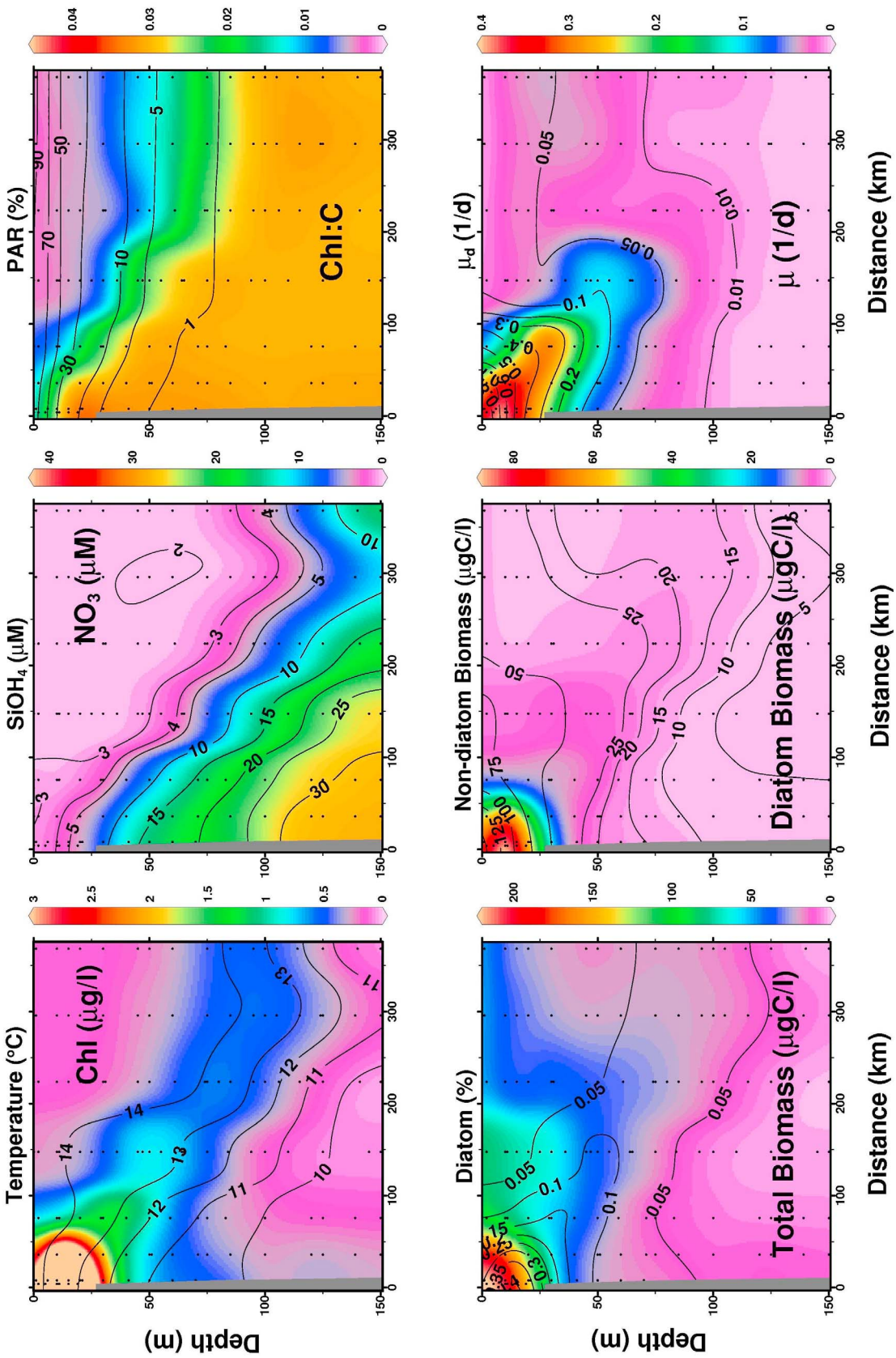

Figure 7. Biogeochemical and biological transect along CalCOFI line 80, from coastal to pelagic waters across the CCS. Colors in each frame are total Chl, NO_3, Chl:C, total C biomass, diatom C biomass, and community growth rate μ. Lines in each frame are temperature, $SiOH_4$, PAR, diatom percentage, nondiatom C biomass, and diatom growth rate μ_d. Temperature, total Chl, $SiOH_4$, and NO_3 are from observations; all other properties are calculated from our model. The location of this section is shown in Figure 1.

monotonically with depth, while the community growth rate showed a weak subsurface maximum offshore, just above the DCM. Both the diatom and bulk community growth rates decreased by about a factor of 10 from inshore to offshore. These growth rates estimated from the CalCOFI section were lower than those found in the CCE study a month later due to the lower nutrient concentrations found across the region during the CalCOFI cruise.

[33] The carbon biomass of phytoplankton can be estimated from measured Chl and the modeled Chl:C ratio. Our model results suggest that the biomass maximum is located near the surface, with a secondary subsurface maximum just above the DCM. Separation of the vertical maxima of biomass and Chl has been observed in many oceans and lakes [*Cullen*, 1982; *Venrick*, 1999; *Fennel and Boss*, 2003] and has been explained as a result of increases in the Chl:C ratio due to acclimation to low light and high nutrients [e.g., *Cullen*, 1982]. Interestingly, our model also showed a second, subsurface peak of carbon biomass close to the DCM, particularly in the offshore stations (Figure 7). Here the high-Chl community contributes substantially to the total water column primary production, similar to patterns observed in subtropical gyres [e.g., *Perez et al.*, 2006]. In the model, the surface biomass maximum is induced largely through light attenuation even without nutrient gradients; the subsurface biomass maximum is generated by a Chl-enriched community growing at the DCM.

[34] Our model predicts that diatoms dominate carbon fixation in upwelling regions, while small nonsiliceous phytoplanktons account for the largest portion of carbon fixation in the pelagic waters. The modeled depth-integrated primary production, estimated from phytoplankton growth rate μ multiplied by its carbon biomass, is 1.7 g C m^{-2} d^{-1} at the coast (near Point Conception) and ~0.10 g C m^{-2} d^{-1} in offshore waters. Unfortunately, there was only one station with C^{14}-based productivity measurements on line 80 during the CalCOFI 0604 cruise. At this station, the observed primary production was 0.20 g C m^{-2} d^{-1} (the half day on-deck incubation value was multiplied by 1.8 to obtain a daily primary production [*Eppley*, 1992]), which compares well with our model estimate of 0.23 g C m^{-2} d^{-1} for the same station. The productivity at a nearby station closest to the Point Conception was 1.6 g C m^{-2} d^{-1}, which also agrees well with the model (1.7 g C m^{-2} d^{-1}). The productivity at the southernmost station measured during cruise 0604 was 0.14 g C m^{-2} d^{-1}. This value is somewhat higher than our model-estimated 0.10 g C m^{-2} d^{-1} but still supports our contention that our model is fairly accurate in reproducing the patterns in phytoplankton growth rate in the CCE.

[35] The contributions of the diatoms and nondiatoms to the productivity and Chl show interesting offshore-onshore patterns. Diatoms comprised ~43% of the integrated total primary production at coastal upwelling zones but less than 2% offshore. However, the contribution of diatoms to the integrated total Chl was somewhat higher: ~51% at the coast and ~5% in pelagic waters. This observation, that large-celled organisms such as diatoms contribute a higher fraction of the total chlorophyll than the total primary production, is consistent with recent observations during the North Atlantic spring phytoplankton bloom [*Pommier et al.*, 2009].

5. Conclusions and Implications

[36] By parameterizing and optimizing a physiology-based model of plankton growth and Chl acclimation, we have demonstrated that the growth rate and Chl:C ratio of phytoplankton can be accurately simulated and predicted in the hydrographically complex southern California Current ecosystem. Our results suggest that the patterns of growth rate are simultaneously determined by nutrients, light, and temperature as well as the phytoplankton community structure. The model can be evaluated using commonly measured properties to diagnose the growth rates and Chl:C ratios of diatoms and nondiatoms, as well as bulk community properties. A model such as this can be easily applied to archived data to quantify long-term trends in phytoplankton growth rates and Chl:C ratios in relation to environmental forcings.

[37] **Acknowledgments.** We thank the LTER-CCE team for their support during the exploration of the southern California Current. Funding of this work comes from NSF-LTER program. Q.P.L. would also like to acknowledge the support of a Scripps Institutional Postdoctoral Award (2007–2009).

References

Armstrong, R. A. (2006), Optimality-based modeling of nitrogen allocation and photoacclimation in photosynthesis, *Deep Sea Res., Part II*, *53*, 513–531.

Behrenfeld, M. J., E. Maranon, D. A. Siegel, and S. B. Hooker (2002), Photoacclimation and nutrient based model of light-saturated photosynthesis for quantifying oceanic primary production, *Mar. Ecol. Prog. Ser.*, *228*, 103–117.

Chai, F., R. C. Dugdale, T.-H. Peng, F. P. Wilkerson, and R. T. Barber (2002), One dimensional ecosystem model of the equatorial pacific upwelling system: Part I. Model development and silicon and nitrogen cycle, *Deep Sea Res., Part II*, *49*, 2713–2745.

Cloern, J. E., C. Grenz, and L. Videgar-Lucas (1995), An empirical model of the phytoplankton chlorophyll:carbon ratio: The conversion factor between productivity and growth rate, *Limnol. Oceanogr.*, *40*, 1313–1321.

Cullen, J. J. (1982), The deep chlorophyll maximum: Comparing vertical profiles of chlorophyll *a*, *Can. J. Fish. Aquat. Sci.*, *39*, 791–803.

DiLorenzo, E., A. J. Miller, N. Schneider, and J. C. McWilliams (2005), The warming of the California Current System: Dynamics, thermodynamics and ecosystem implications, *J. Phys. Oceanogr.*, *35*, 336–362.

Eppley, R. W. (1972), Temperature and phytoplankton growth in the sea, *Fish. Bull.*, *70*, 1063–1085.

Eppley, R. W. (1992), Chlorophyll, photosynthesis and new production in the southern California Bight, *Prog. Oceanogr.*, *30*, 117–150.

Eppley, R.W., F. M. H. Reid, and J. D. H. Strickland (1970), Estimates of phytoplankton crop size, growth rate, and primary production, in *The Ecology of the Plankton Off La Jolla California in the Period April Through September, 1967*, edited by J. D. H. Strickland, vol. 17, pp. 33–42, Bull. Scripps Institution of Oceanography, La Jolla, Calif.

Falkowski, P. G., and J. A. Raven (1999), *Aquatic Photosynthesis*, Blackwell Sci., Malden, Mass.

Fennel, K., and E. Boss (2003), Subsurface maxima of phytoplankton and chlorophyll: Steady state solutions from a simple model, *Limnol. Oceanogr.*, *48*, 1521–1534.

Follows, M. J., S. Dutkiewicz, S. Grant, and S. W. Chisholm (2006), Emergent biogeography of microbial community in a model ocean, *Science*, *315*, 1843–1846.

Franks, P. J. S., J. S. Wroblewski, and G. R. Flierl (1986), Behavior of a simple plankton model with food-level acclimation by herbivores, *Mar. Biol.*, *91*, 121–129.

Garrison, D. L., et al. (2000), Microbial food web structure in the Arabian Sea: A US JGOFS study, *Deep Sea Res.*, *47*, 1387–1422.

Geider, R. J., H. L. MacIntyre, and T. M. Kana (1997), Dynamic model of phytoplankton growth and acclimation: Response of the balanced growth rate and the chlorophyll *a*: Carbon ratio to light, nutrient-limitation and temperature, *Mar. Ecol. Prog. Ser.*, *148*, 187–200.

Geider, R. J., H. L. MacIntyre, and T. M. Kana (1998), A dynamic regulatory model of phytoplanktonic acclimation to light, nutrients, and temperature, *Limnol. Oceangr.*, *45*, 679–694.

Goericke, R. (2002), Top-down control of phytoplankton biomass and community structure in the monsoonal Arabian Sea, *Limnol. Oceanogr.*, *47*, 1307–1323.

Gruber, N., et al. (2006), Eddy-resolving simulation of plankton ecosystem dynamics in the California Current System, *Deep Sea Res., Part I*, *53*, 1483–1516.

Harrison, W. G., and T. Platt (1986), Photosynthesis-irradiance relationships in polar and temperate phytoplankton populations, *Polar Biol.*, *5*, 153–164.

Hutchins, D. A., and K. W. Bruland (1998), Iron-limited diatom growth and Si:N uptake ratios in a coastal upwelling regime, *Nature*, *393*, 561–563.

King, A. L., and K. Barbeau (2007), Evidence for phytoplankton iron limitation in the southern California current system, *Mar. Ecol. Prog. Ser.*, *342*, 91–104.

Kishi, M. J., et al. (2007), NEMURO – A lower trophic level model for the North Pacific marine ecosystem, *Ecol. Model.*, *202*, 12–25.

Landry, M. R., M. D. Ohman, R. Goericke, M. R. Stukel, and K. Tsyrklevich (2009), Lagrangian studies of phytoplankton growth and grazing relationships in a coastal upwelling ecosystem off Southern California, *Prog. Oceanogr.*, *83*, 208–216.

Llewellyn, C. A., J. R. Rishwick, and J. C. Blackford (2005), Phytoplankton community assemblage in the English Channel: A comparison using chlorophyll *a* derived from HPLC-CHEMTAX and carbon derived from microscopy cell counts, *J. Plankton Res.*, *27*, 103–119.

Moisan, J. R., and E. E. Hofmann (1996), Modeling nutrient and plankton processes in the California coastal transition zone 1: A time- and depth-dependent model, *J. Geophy. Res.*, *101*, 22,647–22,676.

Miller, A. J., et al. (1999), Observing and modeling the California Current System, *EOS Trans. AGU*, *80*, 533–539.

Perez, V., et al. (2006), Vertical distribution of phytoplankton biomass, production and growth in the Atlantic subtropical gyres, *Deep Sea Res., Part I*, *53*, 1616–1634.

Platt, T., C. L. Gallegos, and W. G. Harrison (1980), Photoinhibition of photosynthesis in natural assemblages of marine phytoplankton, *J. Mar. Res.*, *38*, 687–701.

Pommier, J., M. Gosselin, and C. Michel (2009), Size-fractioned phytoplankton production and biomass during the decline of the northwest Atlantic spring bloom, *J. Plankton Res.*, *31*, 429–446.

Putland, J. N., and R. L. Iverson (2007), Phytoplankton biomass in a subtropical estuary: Distribution, size composition, and carbon:chlorophyll ratios, *Estuaries and Coasts*, *5*, 1559–2723.

Sherr, E. B., and B. F. Sherr (1993), Preservation and storage of samples for enumeration of heterotrophic protists, in *Current Methods in Aquatic Microbial Ecology*, edited by P. Kemp et al., pp. 207–212, Lewis, NY.

Tian, R. C. (2006), Toward standard parameterizations in marine biological modeling, *Ecol. Model.*, *193*, 363–386.

Valdez-Holguin, J. E., S. Alvarez-Borrego, and B. G. Mitchell (1998), Photosynthetic parameters of phytoplankton in the California Current System, *CalCOFI Rep.*, *39*, 148–158.

Veldhuis, M., and G. Kraay (2004), Phytoplankton in the subtropical Atlantic Ocean: Towards a better assessment of biomass and composition, *Deep Sea Res., Part I*, *51*, 507–530.

Venrick, E. L. (1999), Phytoplankton species structure in the central North pacific, 1973–1996: Variability and persistence, *J. Plankton Res.*, *21*, 1029–1042.

Wang, X. J., M. Behrenfeld, R. LeBorgne, R. Murtugudde, and E. Boss (2009), Regulation of phytoplankton carbon to chlorophyll ratio by light, nutrients and temperature in the equatorial Pacific Ocean: A basin-scale model, *Biogeosciences*, *6*, 391–404.

P. J. S. Franks, R. Goericke, M. R. Landry, Q. P. Li, and A. G. Taylor, Scripps Institution of Oceanography, University of California at San Diego, 9500 Gilman Dr., La Jolla, CA 92093, USA. (qian@coast.ucsd.edu)